

SbsB structure and lattice reconstruction unveil Ca²⁺ triggered S-layer assembly

BARANOVA, Ekatarina; Fronzes, Rémi; Garcia Pino, Abel; Van Gerven, Nani; Papapostolou, David; Péhau-Arnaudet, Gérard; Pardon, Els; Steyaert, Jan; Howorka, Stefan; Remaut, Han Karel

Published in:
Nature

DOI:
[10.1038/nature11155](https://doi.org/10.1038/nature11155)

Publication date:
2012

Document Version:
Final published version

[Link to publication](#)

Citation for published version (APA):

BARANOVA, E., Fronzes, R., Garcia Pino, A., Van Gerven, N., Papapostolou, D., Péhau-Arnaudet, G., ... Remaut, H. K. (2012). SbsB structure and lattice reconstruction unveil Ca²⁺ triggered S-layer assembly. *Nature*, 487, 119-122. <https://doi.org/10.1038/nature11155>

Copyright

No part of this publication may be reproduced or transmitted in any form, without the prior written permission of the author(s) or other rights holders to whom publication rights have been transferred, unless permitted by a license attached to the publication (a Creative Commons license or other), or unless exceptions to copyright law apply.

Take down policy

If you believe that this document infringes your copyright or other rights, please contact openaccess@vub.be, with details of the nature of the infringement. We will investigate the claim and if justified, we will take the appropriate steps.

SbsB structure and lattice reconstruction unveil Ca²⁺ triggered S-layer assembly

Ekaterina Baranova^{1,2}, Rémi Fronzes^{3,4}, Abel Garcia-Pino², Nani Van Gerven^{1,2}, David Papapostolou⁵, Gérard Péhau-Arnaudet⁴, Els Pardon², Jan Steyaert², Stefan Howorka⁵ & Han Remaut^{1,2}

S-layers are regular two-dimensional semipermeable protein layers that constitute a major cell-wall component in archaea and many bacteria^{1–3}. The nanoscale repeat structure of the S-layer lattices and their self-assembly from S-layer proteins (SLPs) have sparked interest in their use as patterning and display scaffolds for a range of nano-biotechnological applications^{4–7}. Despite their biological abundance and the technological interest in them, structural information about SLPs is limited to truncated and assembly-negative proteins^{8–10}. Here we report the X-ray structure of the SbsB SLP of *Geobacillus stearothermophilus* PV72/p2 by the use of nanobody-aided crystallization. SbsB consists of a seven-domain protein, formed by an amino-terminal cell-wall attachment domain and six consecutive immunoglobulin-like domains, that organize into a ϕ -shaped disk-like monomeric crystallization unit stabilized by interdomain Ca²⁺ ion coordination. A Ca²⁺-dependent switch to the condensed SbsB quaternary structure pre-positions intermolecular contact zones and renders the protein competent for S-layer assembly. On the basis of crystal packing, chemical crosslinking data and cryo-electron microscopy projections, we present a model for the molecular organization of this SLP into a porous protein sheet inside the S-layer. The SbsB lattice represents a previously undescribed structural model for protein assemblies and may advance our understanding of SLP physiology and self-assembly, as well as the rational design of engineered higher-order structures for biotechnology^{4–7}.

SLPs (40–200 kDa) self-assemble into paracrystalline lattices that are non-covalently attached to the cell surface, usually by means of one or more N-terminal glycan-binding domains^{1,3,11}. S-layers form a continuous outer protein layer, or exoskeleton, that serves as a protective and/or scaffolding layer, a molecular sieve for nutrient uptake, and a contact zone with the extracellular environment, for example in promoting cell adhesion in pathogenic bacteria such as *Clostridium difficile* and *Bacillus anthracis*^{1,12,13}.

Here we use nanobodies as crystallization chaperones¹⁴ to break the intrinsic self-polymerizing propensity into two-dimensional lattices of the SLP SbsB. We report the 2.4-Å X-ray structure of full-length, mature SbsB (SbsB_{32–920}; residues 32–920) from *Geobacillus stearothermophilus* PV72/p2 (ref. 15), a biophysically¹⁶, biochemically^{17,18} and biotechnologically^{4,19,20} well-characterized SLP (Fig. 1). SbsB is a 98-kDa polypeptide that can be functionally divided into a cell-wall-anchoring N terminus (residues 32–208, consisting of three S-layer homology (SLH) motifs¹⁶) and a carboxy-terminal crystallization region that naturally assembles in an oblique (P1) two-dimensional lattice with the unit-cell vectors $\mathbf{a} = 104 \text{ \AA}$, $\mathbf{b} = 79 \text{ \AA}$ and base angle $\gamma = 81^\circ$ (ref. 19). Nanobodies were raised against an assembly-incompetent SbsB mutant caused by insertion of the haemagglutinin (HA) tag at residue 744 (SbsB_{T744HA})¹⁸. Both the mutant and wild-type SbsB (Supplementary Table 1) were crystallized in complex with nanobody KB6 (NbKB6; Supplementary Fig. 1). The SbsB crystal structure reveals an extended molecule built from

seven distinct domains (domains I–VII; Fig. 1a). The N-terminal 169 amino-acid residues of the mature protein (domain I; residues 32–201), corresponding to the cell-wall attachment domain²¹, are found unresolved in the electron density maps. Domains II (residues 202–292) and III (residues 296–385) are two consecutive C₁-type immunoglobulin folds. Domains IV (residues 391–499), V (residues 502–625) and VI (residues 631–737) are consecutive I-type immunoglobulin folds, and domain VII (residues 738–920) comprises a mixed fold with an immunoglobulin-like β -sandwich core and a random-coil subdomain (residues 769–849) inserted between strands B and C (Fig. 1a and Supplementary Fig. 2).

In the crystal structure, domains II–VII arrange into a disk-like ϕ -shaped quaternary structure 70 Å by 110 Å wide, and 35 Å thick (Fig. 1a, b). In this arrangement, domains IV–VII lie in a single plane and form an annular structure that encloses a central cavity about 24 Å in diameter. This cavity is transversed by a nine-residue linker between domains IV and III, which is positioned on the rim of the ring, underneath domain VI (Fig. 1b). Finally, domain II protrudes from the ring structure, giving shape to the ‘leg’ of the ϕ -shaped monomeric unit (Fig. 1a, b). The ϕ -shaped conformation seen in the crystals is also found for the monomeric protein in solution, as shown by overlays with *ab initio* shapes reconstructed from small-angle X-ray scattering (SAXS) curves obtained for the SbsB_{32–920, T744HA}:NbKB6 and SbsB_{209–920, T744HA}:NbKB6 complexes (an N-terminal deletion mutant removing the unresolved domain I) (Fig. 2 and Supplementary Fig. 3). The averaged *ab initio* shapes for SbsB_{32–920, T744HA}:NbKB6 show an additional density near domain II, corresponding to the N-terminal attachment domain, which was found disordered in the X-ray structure. Comparison of the experimental scattering data with calculated curves from molecular models of SbsB_{32–920, T744HA}:NbKB6 with domain I either unstructured or modelled with the *B. anthracis* Sap SLH domain^{10,13} gives fitting χ^2 values of 2.4 and 13.3, respectively (Supplementary Fig. 3), indicating that the N-terminal domain is largely unstructured in the non-polymerized SbsB and/or in the absence of secondary cell wall polymer (SCWP) (Supplementary Fig. 3 and Methods).

The inter-domain and intra-domain contacts in the SbsB quaternary structure are mediated by Ca²⁺ ions (Fig. 1). A first Ca²⁺ (Ca-1) is shared between domains IV and VII and octahedrally coordinated by residues coming from both domains (Fig. 1 and Supplementary Fig. 4). A second Ca²⁺ site (Ca-2; Fig. 1 and Supplementary Fig. 4) is located at the hinge between domains V and VI. A third site, Ca-3, is positioned in an extended loop of domain VI, near the contact zone with domain VII (Fig. 1 and Supplementary Fig. 4). The fourth site, Ca-4, forms an intra-domain bridge in a coil region of domain VII (Fig. 1 and Supplementary Fig. 4). These Ca²⁺ sites assist in the maintenance of inter-domain contacts and thus probably represent important determinants for the SbsB quaternary structure. Chemically denatured SbsB readily refolds and assembles into S-layers on removal of the chaotropic agents, but

¹Structural and Molecular Microbiology, VIB Department of Structural Biology, VIB, Pleinlaan 2, 1050 Brussels, Belgium. ²Structural Biology Brussels, Vrije Universiteit Brussel, Pleinlaan 2, 1050 Brussels, Belgium. ³Unité G5, Biologie structurale de la sécrétion bactérienne, Institut Pasteur, 25–28 rue du Docteur Roux, 75015 Paris, France. ⁴Unité de recherche mixte 3538, Centre national de la recherche scientifique, Institut Pasteur, 25–28 rue du Docteur Roux, 75015 Paris, France. ⁵Department of Chemistry, Institute of Structural and Molecular Biology, University College London, London WC1H 0AJ, UK.

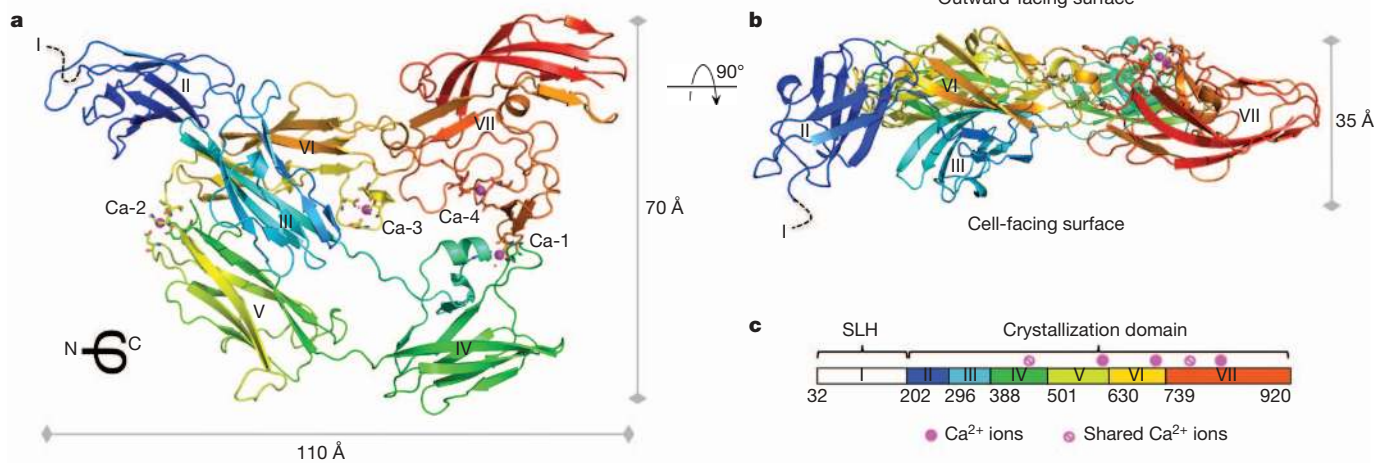


Figure 1 | X-ray structure of *G. stearotheophilus* SbsB. Ribbon representations of the SbsB monomer. **a**, Viewed from the cell-facing side. **(b)** Viewed from inside the plane of the S-layer. SbsB is coloured from blue to red from N terminus to C terminus; Ca^{2+} ions (magenta) and Ca^{2+} -

only in the presence of Ca^{2+} , a characteristic that is shared by many SLPs^{16,22}. Our SAXS data show that EDTA-treated SbsB samples lose quaternary structure (Fig. 2), but the individual domains retain their native secondary structure content as judged by circular dichroism spectra (Fig. 2 inset; thermal denaturation temperatures were 75 and 69 °C in the absence and presence of EDTA, respectively (data not shown)). Thus, Ca^{2+} binding in SbsB triggers a structural transition from an extended chain of folded immunoglobulin domains into a ϕ -shaped quaternary conformation that renders the protein competent for assembly (isothermal titration calorimetry of EDTA or Ca^{2+} titrations reveal Ca^{2+} dissociation constants for the four sites ranging from 0.9 to 110.0 μM ; data not shown). Inter-domain Ca^{2+} binding between neighbouring immunoglobulin domains has previously been observed in cadherins²³. Analogously to SbsB, Ca^{2+} binding in C-cadherin switches the protein structure from a loose rope of consecutive immunoglobulin domains to an active, rigidified hook-like architecture²⁴.

To gain insight into SbsB polymerization, cryo-electron microscopy (cryo-EM) images of SbsB_{209–920} lattices were obtained and combined with the X-ray structure to yield a molecular model of the S-layer. In cryo-EM, the *in vitro* self-assembled lattice of SbsB_{209–920} (Fig. 3a and Supplementary Fig. 5) has unit-cell dimensions $\mathbf{a}^{\text{S-layer}} = 99 \text{ \AA}$, $\mathbf{b}^{\text{S-layer}} = 76 \text{ \AA}$ and base angle $\gamma = 81^\circ$, which are close to the literature values for full-length SbsB from negative-stain electron microscopy ($\mathbf{a} = 104 \text{ \AA}$, $\mathbf{b} = 79 \text{ \AA}$, base angle $\gamma = 81^\circ$)¹⁹. The three-dimensional crystal packing of the SbsB_{32–920}:NbKB6 complex features stacked planes of SbsB layers with pseudotranslational vectors $\mathbf{a}^{\text{X-ray}} = 115.4 \text{ \AA}$, $\mathbf{b}^{\text{X-ray}} = 75.2 \text{ \AA}$ and base angle $\gamma = 72^\circ$, very similar to the S-layer lattice seen in cryo-EM (Fig. 3b). In particular, $\mathbf{b}^{\text{X-ray}}$ seems isomorphous with $\mathbf{b}^{\text{S-layer}}$, whereas $\mathbf{a}^{\text{X-ray}}$ is elongated by 17 \AA and the base angle is shifted by 7° as a result of the inclusion of the nanobody between SbsB monomers (Fig. 3b). We exploited this fortuitous finding of isosymmetry to derive a model for the two-dimensional SbsB lattice in the S-layer. Replacing $\mathbf{a}^{\text{X-ray}}$ with $\mathbf{a}^{\text{S-layer}}$ results in a continuous SbsB lattice, which is maintained through two discrete intermolecular contact zones (Fig. 3c and Supplementary Fig. 6). Along the \mathbf{b} -vector, monomers contact through domains IV and VII, covering a total surface area of 450 \AA^2 , and in agreement with published crosslinking screens¹⁷ (Fig. 3c and Supplementary Fig. 6). Along the calculated \mathbf{a} -vector, the contact is formed through domain II. Overlays with cryo-EM projection maps show the close match of the calculated S-layer model (Fig. 3c and Supplementary Figs 7 and 8). A local discrepancy is seen at domain II, where the projection maps show a displacement of the corresponding density closer towards domain IV

coordinating residues are shown as spheres and sticks, respectively. For clarity, nanobody NbKB6 is not shown. **c**, Schematic representation of the mature SbsB; domains II–VII are coloured as in **a**. Residue numbers indicate domain borders. Magenta dots indicate the locations of Ca^{2+} sites.

of the adjacent molecule (IV^c; Fig. 3c and Supplementary Fig. 8). Molecular dynamics simulations employing intermolecular distance restraints derived from photochemical crosslinking experiments (Fig. 3c and Supplementary Fig. 9) settle domain II in a conformation that coincides with the density observed in the electron microscopy projection maps (Fig. 3c and Supplementary Fig. 8). The modelled position of domain II encompasses a 490 \AA^2 contact surface with the adjacent domain IV and was independently confirmed through Cys–Cys crosslinking of selectively introduced Cys residues in domains II and IV (Fig. 3c and Supplementary Fig. 10). The repositioning of domain II is made possible through a conformational hinge (residues 292–296) with domain III. Between different cryoEM sections, varying levels of electron density are observed for domain II, indicating

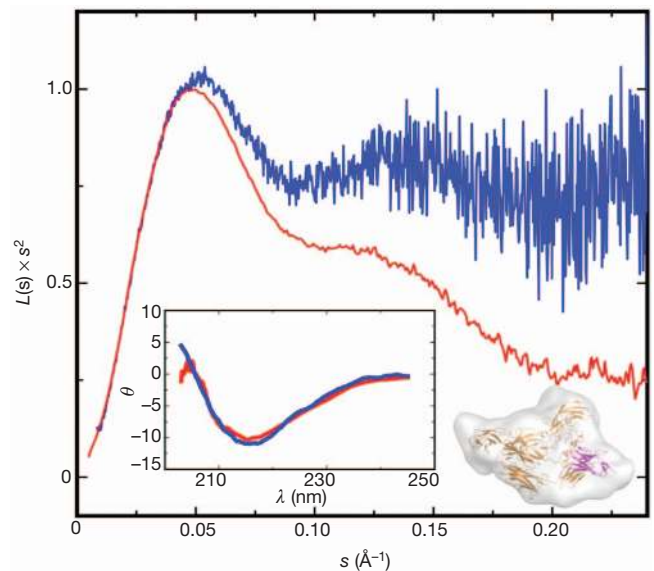


Figure 2 | Solution studies of SbsB quaternary structure. Kratky plots of SbsB_{209–920}:T744HA:NbKB6 before (red) and after the addition of 50 mM EDTA (blue). The native SbsB quaternary structure (averaged *ab initio* shape reconstruction volume is shown in the lower right inset, with SbsB_{209–920}:T744HA and NbKB6 in gold and magenta ribbon, respectively; see Supplementary Fig. 3) is disrupted on the loss of Ca^{2+} , leading to an extended structure consisting of a string of domains II–VII. Under the same conditions, circular dichroism spectra (inset; ellipticity θ is given in units of $10^{-4} \text{ deg cm}^2 \text{ mol}^{-1}$) show that the extended, Ca^{2+} -free protein retains the typical β -sheet conformation, indicating that the individual domains remain folded.

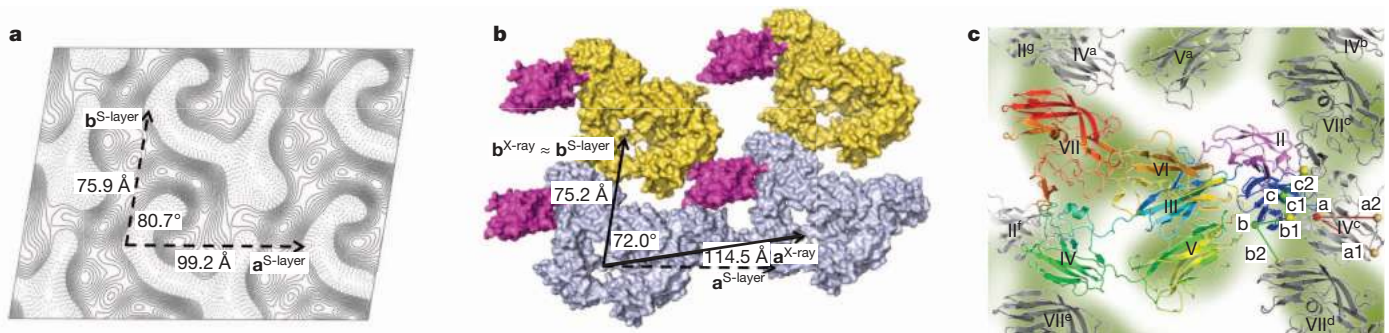


Figure 3 | Cryo-EM imaging and lattice model for the SbsB S-layer.

a, Projection map of *in vitro* grown S-layers of SbsB₂₀₉₋₉₂₀ calculated from a representative image (using a 18 Å resolution cutoff and a $27.0 \times 10^6 \text{ Å}^2$ surface area, corresponding to 3,600 unit cells; Methods and Supplementary Figs 7 and 8; the unit cell is shown as dashed vectors). **b**, Surface representation of SbsB₃₂₋₉₂₀:NbKB6 three-dimensional crystal packing, showing pseudosymmetrical vectors $\mathbf{a}^{\text{X-ray}}$ and $\mathbf{b}^{\text{X-ray}}$, highly similar to $\mathbf{a}^{\text{S-layer}}$ and $\mathbf{b}^{\text{S-layer}}$ (dashed vectors): $\mathbf{b}^{\text{X-ray}}$ and $\mathbf{b}^{\text{S-layer}}$ are isomorphous, whereas the inclusion of NbKB6 (magenta) results in a mismatch between $\mathbf{a}^{\text{X-ray}}$ and $\mathbf{a}^{\text{S-layer}}$. The figure shows two asymmetric units, each containing two SbsB₃₂₋₉₂₀:NbKB6 complexes (orange and blue, with domains II–VII and III–VII ordered, respectively). **c**, Overlay of

cryo-EM projection map (green) with SbsB S-layer model. SbsB₃₂₋₉₂₀ is coloured as in Fig. 1 or in greyscale (light to dark from N terminus to C terminus) for neighbouring protomers (indicated with superscripts a to g). A local mismatch at domain II is resolved by molecular dynamics modelling (X-ray and modelled conformation coloured violet and blue, respectively) using intermolecular distance restraints derived from crosslinking experiments that show that T281C (labelled a) lies within 22 Å of K498 or K499 (red lines labelled a1 and a2). Intermolecular Cys–Cys crosslinking (green lines) of Cys double mutants T240C–K486C (b–b1), T240C–T862C (b–b2), T268C–K486C (c–c1) and T268C–E780C (c–c2) confirms the modelled position for domain II.

that domain II may not adopt a single, uniform conformation throughout the S-layer (Supplementary Fig. 8). This conformational hinge may allow the S-layer to accommodate local topological defects on the bacterial cell surface.

The sidedness with which the modelled S-layer binds the bacterial cell wall (Figs 3 and 4) is assigned by alignment of the lattice vectors with cell-bound or sacculus-bound SbsB lattices¹⁹ and is in excellent

agreement with a previously published accessibility study (Supplementary Fig. 11)^{17,25}. In this topology, domain II is oriented such that the cell-wall-binding domain I is located on the cellular side of the lattice, poised to bind a peptidoglycan-tethered secondary cell-wall polymer²¹. S-layers form a continuous protein sheet wrapping their bacterial cells. Nutrient uptake and cellular secretions require this sheet to be semipermeable. Cryo-EM projections and the modelled SbsB S-layer show zones of perforation in the protein sheet. An intermolecular cavity 30 Å in average diameter and 70 Å in maximum width is formed, lined by domains II, V, VI and VII (Fig. 4).

The bacterial SbsB lattice represents a previously undescribed structural model for two-dimensional protein assemblies. Large spherical or curved assemblies such as viral coats or bacterial polyhedral microcompartments are usually composed of oligomeric protein units that can be structurally tightly integrated^{26–28}. For example, the hexamer of the CA capsid protein from HIV-1 is held together by α -helical bundles as well as by intermolecular donor-helix exchange²⁹. The oligomers facilitate lattice growth by pre-orienting key assembly residues within the oligomeric scaffold. The SbsB lattice, by contrast, is of P1 symmetry and features a monomer as its morphological unit. Two-dimensional lattice formation follows a two-step process with a Ca^{2+} -triggered folding-back of the elongated protein to form a condensed looped quaternary structure. This looped structure prepositions key sites for assembly and renders the protein assembly competent (Fig. 4c). It is likely that the architectural design features of SbsB are applicable to many other SLPs. P1 S-layer lattices and the requirement of Ca^{2+} for assembly are widespread²², and at least for SbsC (17% sequence identity with SbsB) the available structural data show a stretch of multiple immunoglobulin-like domains⁹ (Supplementary Fig. 12). We envisage that the structural insights and the Ca^{2+} -dependent conformational switch in S-layer lattice assembly will provide opportunities for the rational design of dynamic, functionalized coating biomaterials.

METHODS SUMMARY

A set of eight unique SbsB-binding nanobodies, corresponding to three VHH families based on sequence diversity in the CDR2 and CDR3 regions (Supplementary Fig. 1), was generated from a llama (*Llama glama*) immunized with a recombinant SbsB₂₀₉₋₉₂₀:T744HA. Recombinant SbsB₂₀₉₋₉₂₀:T744HA and SbsB₃₂₋₉₂₀ were crystallized with a stoichiometric amount of nanobody NbKB6 and their structures were determined in a single-anomalous-wavelength experiment on a SbsB₃₂₋₉₂₀:T744HA:NbKB6 crystal soaked with 2.5 mM GdCl_3 (Supplementary Table 1). The structure for SbsB₃₂₋₉₂₀:NbKB6 was solved by molecular

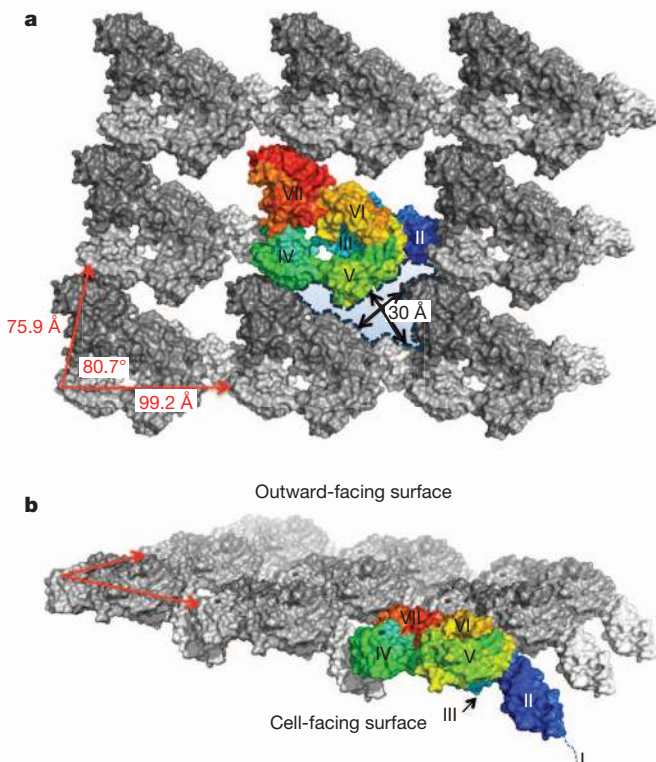


Figure 4 | Model for the *G. stearotherophilus* SbsB S-layer. Surface representation of the modelled SbsB S-layer. **a**, Viewed from the extracellular side. **b**, Tilted in side view. Monomers are coloured in greyscale (light to dark from N terminus to C terminus). For clarity, one monomer is coloured as in Fig. 1. The schematic outline highlights the intermolecular pore formed by three neighbouring subunits. Domain annotation is as in Fig. 1.

substitution and refined to 2.4 Å resolution, providing a model with *R*-factor and free *R*-factor of 18.6% and 23.8%, respectively, and 98% residues in allowed Ramachandran geometry. Circular dichroism spectra were collected at 20 °C on a Jasco J-715 spectropolarimeter, using 200 µl of protein at 0.5 mg ml⁻¹ concentration in buffer A (50 mM Tris-HCl pH 8.0, 150 mM NaCl), with and without 50 mM EDTA. To produce *in vitro* S-layers, purified SbsB_{209–920} at 0.1 mg ml⁻¹ in buffer A supplemented with 2 mM CaCl₂ was concentrated to 1 mg ml⁻¹ and left at 18 °C for a week. Crystals were deposited on glow-discharged carbon-coated 300-mesh grids, flash-frozen in liquid ethane and observed with a Jeol 2010F electron microscope operated at 200 kV. To map residues at the subunit interfaces, SbsB_{T281C} was modified with the photoactivatable and biotin-tagged hetero-bifunctional crosslinker Mts-Atf-LC-biotin, assembled into lattices, and exposed to ultraviolet. Protein dimers were isolated by gel electrophoresis and then digested proteolytically with trypsin. Crosslinked peptide fragments carrying the biotin tag were isolated by affinity purification and subjected to mass spectrometry to determine the peptide mass and sequence (Supplementary Fig. 9).

Full Methods and any associated references are available in the online version of the paper at www.nature.com/nature.

Received 21 December 2011; accepted 19 April 2012.

Published online 10 June 2012.

- Sara, M. & Sleytr, U. B. S-layer proteins. *J. Bacteriol.* **182**, 859–868 (2000).
- Glauert, A. M. The fine structure of bacteria. *Br. Med. Bull.* **18**, 245–250 (1962).
- Messner, P., Schäffer, C., Egelseer, E. M. & Sleytr, U. B. in *Prokaryotic Cell Wall Compounds—Structure and Biochemistry* (eds König, H., Claus, H. & Varma, A.) 53–109 (Springer, 2010).
- Sleytr, U. B. *et al.* in *Progress in Molecular Biology and Translational Science* vol. 103 (ed. Howorka, S.) 277–352 (Academic, 2011).
- Howorka, S. Rationally engineering natural protein assemblies in nanobiotechnology. *Curr. Opin. Biotechnol.* **22**, 485–491 (2011).
- Mark, S. S. *et al.* Bionanofabrication of metallic and semiconductor nanoparticle arrays using S-layer protein lattices with different lateral spacings and geometries. *Langmuir* **22**, 3763–3774 (2006).
- Nam, Y. S. *et al.* Biologically templated photocatalytic nanostructures for sustained light-driven water oxidation. *Nature Nanotechnol.* **5**, 340–344 (2010).
- Fagan, R. P. *et al.* Structural insights into the molecular organization of the S-layer from *Clostridium difficile*. *Mol. Microbiol.* **71**, 1308–1322 (2009).
- Pavkov, T. *et al.* The structure and binding behavior of the bacterial cell surface layer protein SbsC. *Structure* **16**, 1226–1237 (2008).
- Kern, J. *et al.* Structure of surface layer homology (SLH) domains from *Bacillus anthracis* surface array protein. *J. Biol. Chem.* **286**, 26042–26049 (2011).
- Engelhardt, H. & Peters, J. Structural research on surface layers: a focus on stability, surface layer homology domains, and surface layer–cell wall interactions. *J. Struct. Biol.* **124**, 276–302 (1998).
- Calabi, E., Calabi, F., Phillips, A. D. & Fairweather, N. F. Binding of *Clostridium difficile* surface layer proteins to gastrointestinal tissues. *Infect. Immun.* **70**, 5770–5778 (2002).
- Kern, J. & Schneewind, O. BslA, the S-layer adhesin of *B. anthracis*, is a virulence factor for anthrax pathogenesis. *Mol. Microbiol.* **75**, 324–332 (2010).
- Steyaert, J. & Kobilka, B. K. Nanobody stabilization of G protein-coupled receptor conformational states. *Curr. Opin. Struct. Biol.* **21**, 567–572 (2011).
- Sara, M. *et al.* Dynamics in oxygen-induced changes in S-layer protein synthesis from *Bacillus stearothermophilus* PV72 and the S-layer-deficient variant T5 in continuous culture and studies of the cell wall composition. *J. Bacteriol.* **178**, 2108–2117 (1996).
- Runzler, D., Huber, C., Moll, D., Kohler, G. & Sara, M. Biophysical characterization of the entire bacterial surface layer protein SbsB and its two distinct functional domains. *J. Biol. Chem.* **279**, 5207–5215 (2004).
- Kinns, H. & Howorka, S. The surface location of individual residues in a bacterial S-layer protein. *J. Mol. Biol.* **377**, 589–604 (2008).
- Kinns, H., Badelt-Lichtblau, H., Egelseer, E. M., Sleytr, U. B. & Howorka, S. Identifying assembly-inhibiting and assembly-tolerant sites in the SbsB S-layer protein from *Geobacillus stearothermophilus*. *J. Mol. Biol.* **395**, 742–753 (2010).
- Moll, D. *et al.* S-layer–streptavidin fusion proteins as template for nanopatterned molecular arrays. *Proc. Natl Acad. Sci. USA* **99**, 14646–14651 (2002).
- Mader, C., Kupcu, S., Sara, M. & Sleytr, U. B. Stabilizing effect of an S-layer on liposomes towards thermal or mechanical stress. *Biochim. Biophys. Acta* **1418**, 106–116 (1999).
- Sara, M., Egelseer, E. M., Dekitsch, C. & Sleytr, U. B. Identification of two binding domains, one for peptidoglycan and another for a secondary cell wall polymer, on the N-terminal part of the S-layer protein SbsB from *Bacillus stearothermophilus* PV72/p2. *J. Bacteriol.* **180**, 6780–6783 (1998).
- Pavkov-Keller, T., Howorka, S. & Keller, W. in *Progress in Molecular Biology and Translational Science* vol. 103 (ed. Howorka, S.) 73–130 (Academic, 2011).
- Boggon, T. J. *et al.* C-cadherin ectodomain structure and implications for cell adhesion mechanisms. *Science* **296**, 1308–1313 (2002).
- Sotomayor, M. & Schulten, K. The allosteric role of the Ca²⁺ switch in adhesion and elasticity of C-cadherin. *Biophys. J.* **94**, 4621–4633 (2008).
- Howorka, S. *et al.* Surface-accessible residues in the monomeric and assembled forms of a bacterial surface layer protein. *J. Biol. Chem.* **275**, 37876–37886 (2000).
- Li, L., Jose, J., Xiang, Y., Kuhn, R. J. & Rossmann, M. G. Structural changes of envelope proteins during alphavirus fusion. *Nature* **468**, 705–708 (2010).
- Voss, J. E. *et al.* Glycoprotein organization of Chikungunya virus particles revealed by X-ray crystallography. *Nature* **468**, 709–712 (2010).
- Yeates, T. O., Thompson, M. C. & Bobik, T. A. The protein shells of bacterial microcompartment organelles. *Curr. Opin. Struct. Biol.* **21**, 223–231 (2011).
- Ganser-Pornillos, B. K., Cheng, A. & Yeager, M. Structure of full-length HIV-1CA: a model for the mature capsid lattice. *Cell* **131**, 70–79 (2007).

Supplementary Information is linked to the online version of the paper at www.nature.com/nature.

Acknowledgements We thank staff at beamlines Proxima-1 and SWING (SOLEIL), beamline BM30A (European Synchrotron Radiation Facility) and beamline X33 (Deutsches Elektronen-Synchrotron) for technical assistance during data collection. We thank G. Waksman for suggestions on the manuscript, and D. Levy for advice on cryo-EM grid preparation and data collection. This work was supported by VIB (Vlaams Instituut voor Biotechnologie) grant PRJ9 to H.R., the Fonds Wetenschappelijk Onderzoek-Vlaanderen through an Odysseus grant to H.R., a postdoctoral fellowship to A.P.G. and research grant FWO551 to J.S. R.F. is supported by the Centre National de la Recherche Scientifique (CNRS) and the Institut Pasteur. G.P.A. is supported by the CNRS. E.P. received support from Interuniversity Attraction Poles grant P6/19. D.P. was funded by Biotechnology and Biological Sciences Research Council grant BB/E010466/1, and S.H. is grateful for support from University College London. We acknowledge Professor Emeritus U. Sleytr for his lifelong devotion to S-layer protein research and *G. stearothermophilus* SbsB in particular.

Author Contributions K.B. produced and crystallized SbsB:NbKB6 complexes, collected and analysed diffraction and SAXS data and determined their structures. A.P.G. analysed SAXS data and collected SAXS, isothermal titration calorimetry and circular dichroism data. N.V.G. performed mutagenesis and crosslinking experiments. R.F. grew S-layers *in vitro* and analysed cryo-EM data. G.P.A. prepared cryo-EM grids and collected cryo-EM data. E.P. and J.S. produced SbsB-binding nanobodies. D.P. performed crosslinking experiments. S.H. produced SbsB constructs, supervised D.P. and wrote the manuscript. H.R. supervised the work, collected diffraction data, solved and analysed the structures and wrote the manuscript.

Author Information Coordinates and structure factors for SbsB_{32–920}:NbKB6 are deposited in the Protein Data Bank under accession code 4AQ1. Reprints and permissions information is available at www.nature.com/reprints. The authors declare no competing financial interests. Readers are welcome to comment on the online version of this article at www.nature.com/nature. Correspondence and requests for materials should be addressed to H.R. (han.remaut@vib-vub.be).

METHODS

Expression and purification. Nanobodies were expressed as C-terminal His₆ fusions in *Escherichia coli* WK6 periplasm, using the cAb-Lys3-pHEN6 vector³⁰. SbsB_{209–920}, T744HA (containing residues 209–920 of the mature protein), SbsB_{T744HA} and wild-type SbsB were expressed in *E. coli* B834 (DE3) pLysS cytoplasm as fusion products carrying a C-terminal His₆ tag²⁵. Cells expressing NbKB6, grown overnight at 20 °C in lysogeny broth, were washed and incubated for 20 min at 4 °C with the buffer 20 mM Tris/HCl pH 8.0, 20% sucrose, 5 mM EDTA, 0.1 mg ml⁻¹ lysozyme to make spheroplasts. Periplasmic proteins were isolated from spheroplasts by centrifugation (20,000g, 20 min) and dialysed against buffer A (50 mM Tris-HCl pH 8.0, 150 mM NaCl). Pellets from SbsB-expressing cultures were resuspended in buffer A, sonicated and centrifuged for 20 min at 20,000g. Supernatants were mixed with the NbKB6 periplasmic extract, and SbsB:NbKB6 complexes were purified by metal-chelating affinity chromatography employing an imidazole gradient from 40 to 400 mM in buffer A. Remaining protein contaminants and excess NbKB6 were removed by ion-exchange chromatography (HiTrap Q FF; GE Healthcare; buffer: 20 mM Tris-HCl pH 8.0, 40–500 mM NaCl) and hydrophobic interaction chromatography (HiTrap Phenyl HP; GE Healthcare; buffer: 20 mM Tris-HCl pH 8.0, 10 mM NaCl, 1–0 M (NH₄)₂SO₄). No additional Ca²⁺ was added during purification. Our unpublished isothermal titration calorimetry data show that the four Ca²⁺ ions in SbsB have dissociation constants ranging from 0.9 to 110.0 μM. According to ref. 31 the *E. coli* cytoplasm is maintained at 90 ± 10 nM free Ca²⁺, irrespective of extracellular Ca²⁺ levels. Thus, we believe that the protein used for our studies bound Ca²⁺ during cell lysis, when it came in contact with the cellular debris and the pool of cell wall-bound Ca²⁺, which was estimated to be in the range 10–100 mM.

Crystallization and data collection. On purification, wild-type SbsB_{32–920} or SbsB_{209–920} readily aggregates into high-molecular-mass species. To overcome the intrinsic propensity for aggregation or polymerization, wild-type SbsB_{32–920} or SbsB_{209–920} was purified in complex with NbKB6. Purified SbsB:NbKB6 complexes show monodisperse binary complexes that remain stable for days at room temperature and are amenable to three-dimensional crystallization. The role of NbKB6 as a crystallization chaperone is dual. Besides its role in maintaining SbsB in a monodisperse form before crystallization, the nanobody further aids crystallization by providing a contact surface between stacked protein layers inside the three-dimensional crystals (Supplementary Figs 13 and 14). Rod-like crystals (0.5 × 0.07 × 0.05 mm³) of SbsB:NbKB6 complexes (at 9.5 mg ml⁻¹ in 10 mM Tris-HCl pH 8.0, 10 mM NaCl) were obtained by vapour diffusion using 0.2 M potassium isothiocyanate, 0.1 M Bis-Tris propane pH 6.5 and 20% poly(ethylene glycol) 3350. Crystals (in crystallization solution supplemented with 10% (v/v) glycerol) were flash-cooled in liquid nitrogen. Diffraction data for SbsB_{32–920}, T744HA:NbKB6 and SbsB_{32–920}:NbKB6 were collected at 100 K at the PROXIMA-1 beamline at SOLEIL (Saint-Aubin, Essonne, France) and beamline BM30A at the European Synchrotron Radiation Facility (Grenoble, France). Data were integrated and scaled using the XDS package³². The structure of SbsB_{32–920}, T744HA:NbKB6 was solved using a GdCl₃-soaked crystal in a single-anomalous-dispersion experiment at 7,249 eV (Supplementary Table 1). An SbsB_{32–920}, T744HA:NbKB6 crystal was soaked for 90 s in crystallization buffer supplemented with 10% (v/v) glycerol and 2.5 mM GdCl₃ before being flash-cooled in liquid nitrogen. Heavy-atom location (26 Gd³⁺ sites per two SbsB molecules in the asymmetric unit), phase calculation, density modification and initial model building were performed using the Phenix program package³³ and resulted in good-quality electron density maps as judged by the figure of merit (0.51) and the successful autotracing of the two SbsB and two NbKB6 copies in the asymmetric unit. The autotraced models were completed by manual model building using Coot³⁴ and refined to an *R*-factor and free *R*-factor of 31.6% and 36.6%, respectively, using REFMAC5 (ref. 35). The final SbsB structure was refined^{34,35} against data from a native SbsB_{32–920}:NbKB6 crystal collected to 2.4 Å resolution (phased by molecular substitution with the SbsB_{32–920}, T744HA:NbKB6 model), providing a model of 18.6% and 23.6% *R*-factor and free *R*-factor, respectively, containing two copies of NbKB6 (chains B and D) and two SbsB molecules encompassing residues 202–920 (chain A) or residues 295–920 (chain C) and having 98% of residues with ϕ and ψ angles in favoured regions of the Ramachandran diagram (Supplementary Table 1).

SAXS. SAXS data for SbsB_{32–920}, T744HA:NbKB6 and SbsB_{209–920}, T744HA:NbKB6 were collected on the SWING beamline at SOLEIL and beamline X33 at Deutsches Elektronen-Synchrotron (Hamburg, Germany), respectively. Concentrated SbsB_{32–920}, T744HA:NbKB6 (25 μl; 36 mg ml⁻¹ in buffer A) was injected into a size-exclusion column (Shodex KW402.5) and eluted directly into the SAXS flow-through capillary cell at a flow rate of 150 μl min⁻¹. A total of 250 solution scattering curves (each with a 0.5 s recording time) were measured for the main elution peak corresponding to the monomeric protein and were averaged after buffer subtraction. All SAXS curves were measured at 20 °C over the range of

momentum transfer $0.005 < Q = 4\pi \sin(\theta)/\lambda < 0.60 \text{ \AA}^{-1}$, where 2θ is the total scattering angle and $\lambda = 1.5 \text{ \AA}$ is the X-ray wavelength. Samples for SbsB_{209–920}, T744HA:NbKB6 were measured at three concentrations (0.5, 3 and 5 mg ml⁻¹) in buffer A, with and without 50 mM EDTA. Data processing and analysis were performed with PRIMUS³⁶. The radius of gyration R_g and distance distribution function $p(r)$ were calculated using GNOM³⁷. CRY SOL³⁸ was run in default mode (using 50 as the number of degrees of freedom) to generate SAXS curves from the atomic coordinates of the crystallographic structures. Three-dimensional envelopes of SbsB_{T744HA}:NbKB6 and SbsB_{209–920}, T744HA:NbKB6 were calculated *ab initio* from the experimental SAXS curves, using a simulated annealing protocol as implemented in DAMMIF³⁹. SUPCOMB⁴⁰ was used to overlay atomic coordinates on *ab initio* reconstructed shapes and estimate the similarity between models. The reconstructed shapes were very reproducible over the 15 calculated models, and superimposed with average normalized spatial discrepancy value below 1.5. The Ensemble Optimization Method (EOM) implemented in the ATSAS³⁵ suite was used to model the relative orientation and composition of the N-terminal domain. For EOM, domain I was either considered unstructured or modelled using the *B. anthracis* Sap SLH domain^{10,13} as a template. In each implementation this domain was arranged in 10,000 random conformations and the rest of the molecule was fixed with a unique conformation. The fitting of the curves calculated from the modelled ensembles (obtained using both strategies) to the experimental scattering curve suggests that domain I is largely disordered. Volumetric maps were computed from the averaged bead model using the SITUS package⁴¹ and displayed using CHIMERA⁴².

Cryo-electron microscopy. Purified SbsB_{209–920} at 0.1 mg ml⁻¹ in a buffer containing 50 mM Tris-HCl pH 8.0, 150 mM NaCl and 2 mM CaCl₂ was concentrated to 1 mg ml⁻¹ and left at 18 °C for a week. Crystals were then withdrawn and kept at 4 °C. Two-dimensional crystals were adsorbed for 1 min on glow-discharged carbon-coated 300-mesh grids and were flash-frozen in liquid ethane using an automated cryo-plunger (Leica EMPG). The cryo-grids were then transferred to a Jeol 2010F electron microscope operated at 200 kV using a Gatan cryo transfer system (Gatan 626DH). Images were directly assessed using low-electron-dose procedures at a nominal magnification of ×40,000 (real magnification ×54,150) on a 15-μm 4,000 × 4,000-pixel² Gatan charge-coupled device camera corresponding to 2.77 Å per pixel (defocus range 500–1,500 nm).

Cryo-EM images (60 in total) of two-dimensional crystals were treated using the 2dx image processing package⁴³. In brief, the best images (15 in total) were unbled by running two cycles of CCUNBEND. The contrast transfer phase was corrected after the defocus had been determined using CTFIND⁴⁴. The final map was calculated by merging the best images (five images) using 2dx-merge (ref. 45). Projection maps were calculated using programs of the CCP4 package⁴⁶. An isotropic temperature factor ($B = 500$) was applied to compensate for the degradation of image amplitudes. Density contouring was at 0.25 root mean square with densities above the mean contoured by solid lines. The merged projection map was obtained using 123 spots and gave an IQ (signal-to-noise-ratio-based Index of Quality) weighted phase residual of 28.4 on the whole range of the power spectrum (IQ 1–8). The data were filtered at 18 Å to include only high-IQ spots for calculation of the final map (Supplementary Fig. 7).

Mts-Atf-LC-biotin crosslinking experiments. To confirm the location of domain II, a chemical crosslinking procedure (summarized in Supplementary Fig. 9a) was used to identify peptide sequences that in the assembled S-layer lattice of SbsB are proximal (within 22 Å) to the surface-exposed cysteine residue T281C, introduced in domain II. Cell lysates containing His₆-tagged SbsB_{32–920}, T281C (expressed in *E. coli* JM109(DE3)) were loaded on Ni²⁺-nitrilotriacetate resin (600 μl; Qiagen) in buffer B (50 mM NaH₂PO₄, 300 mM NaCl, 10 mM imidazole) supplemented with 0.5 mM dithiothreitol (DTT) (Supplementary Fig. 9a, step 1) and washed three times with prechilled buffer B (600 μl each, in the absence of DTT) to remove non-His₆-tagged protein. The column-bound protein (about 250 μg) was chemically modified with the thiol-reactive moiety of the heterobifunctional, photoactivatable and biotin-tagged crosslinker Mts-Atf-LC-biotin (Pierce) by a 20-min incubation (under subdued light) at 4 °C in 500 μM crosslinker in buffer B (Supplementary Fig. 9a, step 2). Excess reagent was removed by short centrifugation, followed by four washes with prechilled buffer B (600 μl each). The modified protein was eluted in buffer B supplemented with 250 mM imidazole and mixed with a freshly prepared suspension of peptidoglycan sacculi of *G. stearothermophilus* PV72/p2 (3:1 weight ratio of eluted SbsB protein to peptidoglycan sacculi) and incubated overnight at 4 °C, yielding S-layer assembly products as shown by negative staining and transmission electron microscopy (Supplementary Fig. 9a, step 3). The photosensitive azidotrifluorophenyl-moiety (Atf) of Mts-Atf-LC-biotin-modified SbsB_{32–920}, T281C was activated by exposure to ultraviolet (360 nm for 15 min at a distance of 2–5 cm from the solution) leading to the formation of a covalent bond between the crosslinker and an accessible lysine residue within 22 Å distance range (Supplementary Fig. 9a,

step 4). Unreacted crosslinker was quenched by adding 20 μl of 1.5 M Tris-HCl pH 8.0. SbsB dimers and monomers, corresponding to intramolecularly and intermolecularly reacted species, respectively, were isolated by SDS-PAGE (7.5% bisacrylamide gels) (Supplementary Fig. 9a, step 5). The Coomassie-blue-stained gel bands were cut out and destained with an aqueous solution containing 5% methanol and 7% acetic acid. After removing the destaining solution, the gel slices were further purified by rinsing with acetonitrile and water, followed by incubation for 30 min with a mixture of freshly prepared 50% $(\text{NH}_4)_2\text{CO}_3$ buffer in acetonitrile at 37 °C under gentle shaking, and dried. SbsB protein was subjected to proteolytic digestion by swelling the dried gel slices in a 10 $\text{ng}\mu\text{l}^{-1}$ solution of trypsin (40 μl ; NEB; catalogue no. P8101S) in reaction buffer (50 mM Tris-HCl pH 8.0, 20 mM CaCl_2) for 20 min, followed by the addition of reaction buffer to cover the slice and incubation overnight at 25 °C under gentle shaking (Supplementary Fig. 9a, step 6). The digestion reaction was stopped by the addition of phenylmethylsulphonyl fluoride to a final concentration of 1 mM. Crosslinked peptides were purified from the supernatant by incubation for 45 min at room temperature with streptavidin-agarose beads (20 μl ; Pierce) equilibrated in PBS buffer, supplemented with 10 mM DTT to cleave the disulphide bond between the cysteine-bearing peptide and the peptide containing the Atf-reacted Lys (Supplementary Fig. 9a, step 7). The affinity-bound peptides were eluted by the addition of 0.1% trifluoroacetic acid in ultrapure water (20 μl) followed by centrifugation (Supplementary Fig. 9a, step 8). The sequence identity of the chemically modified peptide was identified using matrix-assisted laser desorption/ionization mass spectrometry (MALDI-MS) using a Waters MALDI microMX instrument in the reflectron positive or linear positive mode, from 1,200 m/z to 5,000 m/z (Supplementary Fig. 9b, c). The MS traces of SbsB₃₂₋₉₂₀, T281C and wild-type SbsB protein were compared, to identify peaks specific for the crosslinked proteins (Supplementary Fig. 9b). In addition, MS traces for monomeric and dimeric protein were compared, to pinpoint unique major signals (Supplementary Fig. 9b). The m/z values of the identified peaks were then corrected by subtracting the mass of the fragment of the chemical crosslinker (847.02 Da) to yield the peptide mass. The corresponding peptide sequence was inferred by matching the mass to the predicted peptide fragments obtained from the MS-Digest server at the University of California, San Francisco (<http://prospector.ucsf.edu/prospector/mshome.htm>) and allowing for adducts of Na^+ . Results are summarized in Supplementary Fig. 9c.

Molecular dynamics simulations. Molecular dynamics simulations were performed with the software Almost (<http://www.open-almost.org>). Starting from the reconstituted S-layer (Fig. 3c), a pair of SbsB₂₀₉₋₉₂₀ molecules corresponding to the intermolecular contact zone along the S-layer *a* axis was selected (representing the interface between domains II and IV^c; Fig. 3c). An ensemble of structures was generated with domain II randomly oriented with respect to the rest of the domains. Short torsion-angle molecular dynamics simulations (100 ps) were run to ensure that the structures did not contain distorted bond angles. We then used a 22 Å distance cutoff between atom SG of residue T281C and the NZ atom of K498 or K499 in domain IV of the adjacent SbsB monomer to select an initial set of structures for molecular dynamics calculations, run using the Amber03 force field⁴⁷ in stages of 500 steps with step sizes of 0.002 ps for a total of about 1.0 ns. An ensemble of the top ten energy-minimized structures shows an average root mean square deviation of 1.1 Å for the equivalent C α atoms in domain II, showing that the modelling strategy resulted in one discrete conformation for domain II. A representative structure from this ensemble was used to calculate the S-layer model shown in Figs 3c and 4, using the vector replacement method described above.

BM(PEG)₃ crosslinking. On the basis of the modelled position of domain II, SbsB₂₀₀₋₉₂₀ double Cys mutants were made that introduced a surface-exposed

Cys on either side of the intermolecular interface. Cys substitutions were chosen to lie within 18 Å of one another such that they could be crosslinked with the thiol-reactive homo-bifunctional crosslinker BM(PEG)₃ (Pierce; BM(PEG)₃ holds two maleimide groups spaced 17.8 Å apart). In this way, four double mutants were generated: T240C/K486 (II/IV^c: 15.9 Å), T240C/T862C (II/VII^c: 16.9 Å), T268C/K486C (II/IV^c: 9.4 Å) and T268C/E780C (II/IV^d: 17.0 Å) (Fig. 3c and Supplementary Fig. 10). His₆-tagged SbsB₂₀₀₋₉₂₀ double mutants were purified by nickel-affinity chromatography. SbsB₂₀₀₋₉₂₀ mutants were eluted in PBS containing 1 M imidazole and 10 mM DTT to avoid Cys oxidation; they were spin-concentrated to 50 μM , washed twice in PBS, 10 mM DTT, 1 mM CaCl_2 before incubation overnight at 4 °C to allow S-layer formation. S-layers were then separated from soluble protein by centrifugation (20,000g, 15 min), washed twice with PBS to remove DTT and resuspended in PBS to a final concentration of 40 μM before the addition of threefold molar excess BM(PEG)₃. After incubation for 60 min at room temperature, non-reacted BM(PEG)₃ was quenched by the addition of 50 mM DTT. Non-crosslinked polymers were redissolved by the addition of 20 mM EDTA, 2.5 M urea, before being loaded on SDS-PAGE gels for analysis (Supplementary Fig. 10; loading buffer contained 100 mM 2-mercaptoethanol to reduce oligomers that might have formed as a result of Cys oxidation).

- De Genst, E. *et al.* Chemical basis for the affinity maturation of a camel single domain antibody. *J. Biol. Chem.* **279**, 53593–53601 (2004).
- Gangola, P. & Rosen, B. P. Maintenance of intracellular calcium in *Escherichia coli*. *J. Biol. Chem.* **262**, 12570–12574 (1987).
- Kabsch, W. Integration, scaling, space-group assignment and post-refinement. *Acta Crystallogr. D Biol. Crystallogr.* **66**, 133–144 (2010).
- Adams, P. D. *et al.* PHENIX: a comprehensive Python-based system for macromolecular structure solution. *Acta Crystallogr. D Biol. Crystallogr.* **66**, 213–221 (2010).
- Emsley, P. & Cowtan, K. Coot: model-building tools for molecular graphics. *Acta Crystallogr. D Biol. Crystallogr.* **60**, 2126–2132 (2004).
- Murshudov, G. N. *et al.* REFMAC5 for the refinement of macromolecular crystal structures. *Acta Crystallogr. D Biol. Crystallogr.* **67**, 355–367 (2011).
- Konarev, P., Volkov, V. V., Sokolova, A. V., Koch, M. H. J. & Svergun, D. I. PRIMUS: a Windows PC-based system for small-angle scattering data analysis. *J. Appl. Cryst.* **36**, 1277–1282 (2003).
- Svergun, D. I. Determination of the regularization parameter in indirect-transform methods using perceptual criteria. *J. Appl. Cryst.* **25**, 495–503 (1992).
- Svergun, D. I., Barberato, C. & Koch, M. H. J. CRYSOLE—a program to evaluate X-ray solution scattering of biological macromolecules from atomic coordinates. *J. Appl. Cryst.* **28**, 768–773 (1995).
- Svergun, D. I., Petoukhov, M. V. & Koch, M. H. Determination of domain structure of proteins from X-ray solution scattering. *Biophys. J.* **80**, 2946–2953 (2001).
- Kozin, M. B. & Svergun, D. I. Automated matching of high- and low-resolution structural models. *J. Appl. Cryst.* **34**, 33–41 (2001).
- Wriggers, W. Using Situs for the integration of multi-resolution structures. *Biophys. Rev.* **2**, 21–27 (2010).
- Pettersen, E. F. *et al.* UCSF Chimera—a visualization system for exploratory research and analysis. *J. Comput. Chem.* **25**, 1605–1612 (2004).
- Gipson, B., Zeng, X., Zhang, Z. Y. & Stahlberg, H. 2dx—user-friendly image processing for 2D crystals. *J. Struct. Biol.* **157**, 64–72 (2007).
- Mindell, J. A. & Grigorieff, N. Accurate determination of local defocus and specimen tilt in electron microscopy. *J. Struct. Biol.* **142**, 334–347 (2003).
- Gipson, B., Zeng, X. & Stahlberg, H. 2dx_merge: data management and merging for 2D crystal images. *J. Struct. Biol.* **160**, 375–384 (2007).
- Collaborative Computational Project Number 4. The CCP4 suite: programs for protein crystallography. *Acta Crystallogr. D Biol. Crystallogr.* **50**, 760–763 (1994).
- Duan, Y. *et al.* A point-charge force field for molecular mechanics simulations of proteins based on condensed-phase quantum mechanical calculations. *J. Comput. Chem.* **24**, 1999–2012 (2003).